Nanoscale subsurface imaging via resonant difference-frequency atomic force ultrasonic microscopy

Sean A. Cantrell,[a] John H. Cantrell,[b] and Peter T. Lillehei[c]
Research and Technology Directorate, NASA Langley Research Center, Hampton, Virginia 23681

A scanning probe microscope methodology, called resonant difference-frequency atomic force ultrasonic microscopy (RDF-AFUM), has been developed. It employs an ultrasonic wave launched from the bottom of a sample while the cantilever of an atomic force microscope, driven at a frequency differing from the ultrasonic frequency by one of the contact resonance frequencies of the cantilever, engages the sample top surface. The nonlinear mixing of the oscillating cantilever and the ultrasonic wave in the region defined by the cantilever tip–sample surface interaction force generates difference-frequency oscillations at the cantilever contact resonance. The resonance-enhanced difference-frequency signals are used to create images of nanoscale near-surface and subsurface features. An analytical model is presented for assessing the RDF-AFUM phase signal resulting from near-surface variations in the sample contact stiffness and from the interaction of the bulk wave with subsurface structures. The application of the model to RDF-AFUM phase measurements of a 12.7 μm thick film of LaRC™-CP2 polyimide polymer containing a monolayer of gold nanoparticles embedded 7 μm below the specimen surface reveals variations in the Young modulus of the material of approximately 24% over regions roughly 10–35 nm wide. The magnitude of the modulus variations suggests the occurrence of contiguous amorphous and crystalline phases within the bulk of the polymer. The RDF-AFUM micrograph indicates a preferential growth of the crystalline phase in the vicinity of the gold nanoparticles. [DOI: 10.1063/1.2743908]

I. INTRODUCTION

The rapid development of new materials produced by the embedding of nanostructural constituents into matrix materials has placed increased demands on the development of new measurement methods and techniques to assess the microstructure-physical property relationships of such materials. Although a number of techniques are available for near-surface characterization, methods to assess deeper (subsurface) features at the nanoscale remain largely in development. Several successful efforts at nanoscale subsurface imaging have involved combining the lateral resolution of the atomic force microscope[1] (AFM) with the nondestructive capability of acoustic methodologies.[2–13] The utilization of the AFM, in principle, provides the necessary lateral resolution for obtaining subsurface images at the nanoscale, but the AFM alone does not enable subsurface imaging. The propagation of acoustic waves through the bulk of the specimen and the impinging of those waves on the specimen surface in contact with the AFM cantilever enable such imaging. The use of acoustic waves in the ultrasonic range of frequencies more optimally takes advantage of this resolution since both the intensity and the phase variation of waves scattered from nanoscale structures increase with increasing frequency.[14] A basic problem with probing at ultrasonic frequencies, however, is the reduced response of the AFM cantilever relative to that at lower frequencies.

To avoid the reduced cantilever response at ultrasonic frequencies, Cuberes *et al.*[11] and Shekhawat and Dravid[12] have developed methodologies that utilize difference frequencies generated at the surface of a specimen by the interaction of ultrasonic waves incident from below the surface and high frequency oscillations of the AFM cantilever. In both cases the ultrasonic and cantilever driving frequencies are set to generate a difference-frequency signal that is well below the lowest resonant vibrational frequency of the cantilever. The method of Shekhawat and Dravid[12] requires modification of the AFM to implement, and they explained that their difference-frequency signal results from a simple linear beating of interacting sinusoidal signals. We introduce a modification of the approaches of Cuberes *et al.* and Shekhawat and Dravid that makes direct use of contact resonances of the AFM cantilever to enhance the signal output. A description of the present technique, called resonant difference-frequency atomic force ultrasonic microscopy (RDF-AFUM), is given in Sec. II.

An analytical model is developed in Sect. III for the RDF-AFUM output signal resulting from the interaction of the ultrasonic wave generated at the bottom of the sample with nano-/microstructural features within the sample bulk material and from nonlinear cantilever tip–sample surface interactions. An application of the analytical model to the quantitative assessment of the variations in the Young moduli within the bulk of a 12.7 μm thick layer of LaRC™-CP2

[a]Present address: Department of Physics, University of Virginia, Charlottesville, VA 22904; electronic mail: sac3k@virginia.edu
[b]Electronic mail: john.h.cantrell@nasa.gov
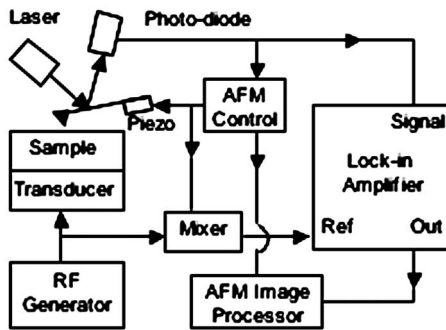[c]Electronic mail: peter.t.lillehei@nasa.gov

FIG. 1. Schematic of equipment arrangement for the resonant difference-frequency atomic force ultrasonic microscope (RDF-AFUM).

polyimide polymer is presented in Sec. IV using the results of RDF-AFUM measurements. The polymer contains a monolayer of 10–15 nm diameter gold particles embedded 7 μm below the film surface.

II. RESONANT DIFFERENCE-FREQUENCY ATOMIC FORCE ULTRASONIC MICROSCOPY

RDF-AFUM employs an ultrasonic wave launched from the bottom of a sample, while the cantilever of an atomic force microscope, driven at a frequency differing from the ultrasonic frequency by one of the contact resonance frequencies of the cantilever, engages the sample top surface. It is important to note that at high drive amplitudes of the ultrasonic wave or cantilever (or both) the contact resonance frequency may also include a nonlinear oscillation mode of the cantilever. The nonlinear mixing of the oscillating cantilever and the ultrasonic wave in the region defined by the cantilever tip–sample surface interaction force generates difference-frequency oscillations at the cantilever contact (linear or nonlinear) resonance. Variations in the amplitude and phase of the bulk wave due to the presence of subsurface nano-/microstructures as well as variations in near-surface material parameters affect the amplitude and phase of the difference-frequency signal. These variations are used to create spatial mappings generated by subsurface and near-surface structures.

A schematic of the RDF-AFUM equipment arrangement is shown in Fig. 1. A Veeco Instruments Nanoscope IV MultiMode AFM is used for the control and processing of the images. The commercial AFM cantilever used in the present work is measured to have a flexural stiffness modulus of 14 N m^{-1} and a fundamental resonance of 302 kHz. An HP model 3325A function generator is used to deliver a 1.8 MHz sinusoidal driving signal to a narrow-band piezoelectric transducer (PZT) bonded to the surface of the sample opposite the cantilever. A drive signal is sent to the cantilever, operating in an intermittent soft contact mode, from the AFM control box to a broadband piezostack under the cantilever. The cantilever drive frequency, the amplitude, and the cantilever tip–sample surface separation are varied until the difference between the ultrasonic wave and cantilever drive frequencies correspond to a contact (linear or nonlinear) resonance of the cantilever. In the present experiment a cantilever drive frequency of 2.1 MHz, together with the 1.8 MHz ultrasonic drive frequency, generates a difference-

frequency signal of approximately 0.3 MHz, corresponding to a nonlinear contact resonance of the cantilever. The frequency of the nonlinear contact resonance serendipitously corresponds very nearly to that of the lowest order linear noncontact resonance frequency of the cantilever.

The cantilever drive and transducer drive signals are split and fed to a mixer. The mixer output signal, consisting of sum- and difference-frequency signals, is sent to the reference input of a PAR model 5302 lock-in amplifier that, because of its limited bandpass, filters out the sum frequency. The AFM photodiode signal, derived from the cantilever response from all sources, is then sent to the signal input of the lock-in amplifier where all frequencies except the difference-frequency are filtered out. The lock-in amplifier measures both the amplitude and phase of the input difference-frequency signal. The appropriate output signal from the lock-in amplifier is fed to the AFM processor to build up either amplitude or phase images as the sample is scanned.

Before commencing a scan, it is useful to determine the setpoint value of the feedback parameter that maximizes the amplitude of the difference-frequency signal. The intermittent soft contact mode may be operated while holding one of three parameters constant in the AFM feedback loop: (1) the quiescent deflection of the cantilever, (2) the amplitude of the cantilever's response to the piezodrive signal ("normal" amplitude), and (3) the phase lag between the cantilever's response to the piezodrive signal and the drive signal itself (normal phase). Calibration curves are taken in which the values of each of these possible feedback parameters are plotted together with the difference-frequency amplitude as a function of the cantilever tip–sample surface separation. From these curves a feedback parameter and a setpoint value are chosen to coincide with the maximum difference-frequency signal. Generally, the normal amplitude produces the most stable difference-frequency signal when used as the feedback parameter.

As the cantilever tip engages the sample surface, it encounters an interaction force that varies nonlinearly with the tip-surface separation distance. The deflection of the cantilever obtained in calibration plots is related to this force. For small slopes of the deflection versus separation distance, the interaction force and cantilever deflection curves are approximately related via a constant of proportionality. The maximum difference-frequency signal amplitude occurs when the quiescent deflection of the cantilever approaches the bottom of the force well, where the maximum change in the slope of the force versus separation curve (hence, maximum interaction force nonlinearity) occurs.

III. MODEL OF RDF-AFUM SIGNAL GENERATION

The above description of RDF-AFUM provides that the difference-frequency signal results from the nonlinear interaction force between the oscillating cantilever tip and the sample surface vibrating in response to incident ultrasonic bulk waves generated at the bottom of the sample. It is assumed that image contrast is dominated by two principal contributions to the difference-frequency signal: (1) the variations in the amplitude and phase of the ultrasonic wave

resulting from features within the sample bulk and (2) the effects of variations in the sample surface contact stiffness on the nonlinear cantilever tip–sample surface interactions. This assumption is based on the results of a detailed analytical model we have developed of the general cantilever response to the nonlinear cantilever tip–sample surface interactions for a variety of acoustic-atomic force modalities. The model is too long to reproduce here and is the subject of a manuscript in preparation for journal submission.[15] However, a feasibility argument that leads to the most important results may be given.

We begin with an assessment of a continuous ultrasonic wave propagating through a material of finite thickness and the variations in amplitude and phase of the wave resulting from structural features embedded within the bulk of the sample. As the ultrasonic wave impinges upon the sample surface, it mixes with the cantilever oscillations via the nonlinear tip-surface interaction force to generate a difference-frequency signal. The amplitude and phase variations generated in the bulk material are carried to the sample surface by the propagating ultrasonic wave and become an integral part of the ultrasonic wave contribution to variations in the difference-frequency signal. This aspect of the model is based on the propagating wave model of Bolef and Miller.[16] Sample near-surface features also contribute to the difference-frequency signal via the effect of the contact stiffness associated with such features directly on the nonlinear cantilever tip–sample surface interaction itself. The near-surface contributions include not only those produced at the cantilever drive frequency and manifested in the difference-frequency signal via the nonlinear tip-surface interaction but also those generated by the difference-frequency drive signal itself.

A. Variations in signal amplitude and phase from subsurface features

We consider a traveling stress wave of unit amplitude of the form $e^{-\alpha x}\cos(\omega_s t - kx) = \mathrm{Re}[e^{-\alpha x}e^{i(\omega_s t - kx)}]$, where α is the attenuation coefficient, x is the propagation distance, ω_s is the angular frequency, t is time, $k = \omega_s/c$, and c is the phase velocity, propagating through a sample of thickness $a/2$. We assume that the wave is generated at the bottom surface of the sample at the position $x=0$ and that the wave is reflected between the top and bottom surfaces of the sample. We assume that the effect of the reflections is simply to change the direction of wave propagation; changes in the sign of the wave amplitude at each reflection produce an inconsequential phase shift in the final results.

For continuous waves the complex wave form at a point x in the material consists of the sum of all contributions resulting from waves which had been generated at point $x=0$ and have propagated to point x after multiple reflections from the sample boundaries. We thus write the complex wave $\widetilde{A}(t)$ as

$$\widetilde{A}(t) = e^{-\alpha x}e^{i(\omega_s t - kx)}[1 + e^{-(\alpha a + ika)} + \cdots + e^{-N(\alpha a + ika)} + \cdots]$$

$$= e^{-\alpha x}e^{i(\omega_s t - kx)}\sum_{N=0}^{\infty}[e^{-(\alpha a + ika)}]^N$$

$$= e^{-\alpha x}e^{i(\omega_s t - kx)}\frac{1}{1 - e^{-(\alpha a + ika)}}, \qquad (1)$$

where the last equality follows from the geometric series generated by the infinite sum. The real wave form $A(t)$ is obtained from Eq. (1) as

$$A(t) = \mathrm{Re}[\widetilde{A}(t)] = e^{-\alpha x}(A_1^2 + A_2^2)^{1/2}\cos(\omega_s t - kx - \phi)$$

$$= e^{-\alpha x}B\cos(\omega_s t - kx - \phi) \qquad (2)$$

where

$$A_1 = \frac{e^{\alpha a} - \cos ka}{2(\cosh \alpha a - \cos ka)}, \qquad (3)$$

$$A_2 = -\frac{\sin ka}{2(\cosh \alpha a - \cos ka)}, \qquad (4)$$

$$\phi = \tan^{-1}\frac{\sin ka}{e^{\alpha a} - \cos ka}, \qquad (5)$$

and

$$B = (A_1^2 + A_2^2)^{1/2} = (1 + e^{-2\alpha a} - 2e^{-\alpha a}\cos ka)^{-1/2}. \qquad (6)$$

The evaluation (detection) of a continuous wave at the end of the sample opposite that of the source is obtained by setting $x=a/2$ in the above equations. It is at $x=a/2$ that the AFM cantilever engages the sample surface. In the following equations we set $x=a/2$.

The above results are derived for a homogeneous specimen. Consider now that the specimen of thickness $a/2$ having a phase velocity c contains an embedded material of thickness $d/2$ having a phase velocity c_d. The phase factor $ka = \omega_s a/c$ in Eqs. (2)–(6) must then be replaced by $ka - \psi$, where

$$\psi = \omega_s d\left(\frac{1}{c} - \frac{1}{c_d}\right) = \omega_s d\frac{\Delta c}{c_d c} = kd\frac{\Delta c}{c_d}, \qquad (7)$$

where $\Delta c = c_d - c$. We thus set $x=a/2$ and rewrite Eqs. (2), (5), and (6) as

$$A'(t) = e^{-\alpha a/2}B'\cos\left[\omega_s t - \frac{(ka - \psi)}{2} - \phi'\right], \qquad (8)$$

where

$$\phi' = \tan^{-1}\frac{\sin(ka - \psi)}{e^{\alpha a} - \cos(ka - \psi)} \qquad (9)$$

and

$$B' = [1 + e^{-2\alpha a} - 2e^{-\alpha a}\cos(ka - \psi)]^{-1/2}. \qquad (10)$$

We have assumed in obtaining the above equations that the change in the attenuation coefficient resulting from the embedded material is negligible.

For small ψ we may expand Eq. (9) in a power series about $\psi=0$. Keeping only terms to first order, we obtain

$$\phi' = \phi + \Delta\phi, \tag{11}$$

where

$$\Delta\phi = -\psi\left[\frac{e^{\alpha a}\cos ka - 1}{(e^{\alpha a} - \cos ka)^2 + \sin^2 ka}\right]. \tag{12}$$

Equation (8) is thus approximated as

$$A'(t) = e^{-\alpha a/2}B'\cos\left(\omega_s t - \frac{ka}{2} - \phi + \frac{\psi}{2} - \Delta\phi\right)$$

$$= e^{-\alpha a/2}B'\cos(\omega_s t + \theta), \tag{13}$$

where

$$\theta = -(\chi + \Delta\chi) = -\left(\frac{ka}{2} + \phi - \frac{\psi}{2} + \Delta\phi\right), \tag{14}$$

where

$$\chi = \frac{ka}{2} + \phi \tag{15}$$

and

$$\Delta\chi = -\frac{\psi}{2} + \Delta\phi = -\psi\left[\frac{1}{2} + \frac{e^{\alpha a}\cos ka - 1}{(e^{\alpha a} - \cos ka)^2 + \sin^2 ka}\right]. \tag{16}$$

Equation (13) reveals that the total phase contribution at $x = a/2$ is θ, and from Eqs. (14) and (16) the phase variation resulting from the embedded material is $-\Delta\chi$.

The fractional change in the Young modulus $\Delta E/E$ is related to the fractional change in the ultrasonic longitudinal velocity $\Delta c/c$ as $\Delta E/E \approx \Delta C_{11}/C_{11} = (2\Delta c/c) + (\Delta\rho/\rho)$, where ρ is the mass density of the sample and C_{11} is the Brugger longitudinal elastic constant. Assuming that the fractional change in the mass density is small compared to the fractional change in the wave velocity, we may estimate the relationship between $\Delta E/E$ and $\Delta c/c$ as $\Delta E/E \approx 2\Delta c/c$. This relationship may be used to express ψ, given in Eq. (7) in terms of $\Delta c/c_d = (c/c_d)(\Delta c/c)$, in terms of $\Delta E/E$.

B. Contributions from nonlinear cantilever tip–sample surface interactions

In addition to that from the embedded material, a phase shift in the RDF-AFUM signal occurs directly from the nonlinear cantilever tip–sample surface interaction that generates an effective driving force for sample surface oscillations at the difference frequency. The surface contributions include not only those produced at the cantilever drive frequency and manifested in the difference-frequency signal via the nonlinear tip-surface interaction, but also those generated by an effective difference-frequency drive signal itself. The phase shift at the difference frequency generated by the effective difference-frequency drive signal itself may be obtained by considering that the small mass m_s of the sample material involved in the cantilever-sample tip interaction obeys to a good approximation the damped harmonic oscillator equation

$$m_s\ddot{z} + \gamma_s\dot{z} + [k_s + F'(z_0)]z = F\cos(\Delta\omega)t = \mathrm{Re}[Fe^{i(\Delta\omega)t}], \tag{17}$$

where the difference frequency $\Delta\omega = (\omega_c - \omega_s)$, ω_c is the cantilever frequency, ω_s is the ultrasonic frequency, γ_s is the damping coefficient, k_s is the sample contact stiffness constant, F is the amplitude of the driving force, z is the instantaneous tip-surface separation distance, and $F'(z_0)$ is the effective stiffness constant of the nonlinear interaction force at the quiescent cantilever tip–sample surface separation distance z_0.

When the quiescent separation distance z_0 is less than (greater than) that corresponding to the bottom of the force-separation curve, $F'(z_0)$ is negative (positive). When operating in the nonlinear interaction (soft contact) region of the cantilever tip–sample surface force-separation curve, $F'(z_0)$ is generally small compared to that of the hard tip-surface contact region but can be significant in the RDF-AFUM signal calculations, especially for small values of k_s and cantilever stiffness constant k_c. Assuming that the mass m_s is negligibly small, we obtain the steady state solution to Eq. (17) to be

$$z = \mathrm{Re}\left(\frac{Fe^{i(\Delta\omega)t}}{k_s + F'(z_0) + i\gamma_s\Delta\omega}\right)$$

$$= \frac{F}{[(k_s + F'(z_0))^2 + \gamma_s^2(\Delta\omega)^2]^{1/2}}\cos[(\Delta\omega)t - \beta_{cs}], \tag{18}$$

where

$$\beta_{cs} = \tan^{-1}\frac{\gamma_s\Delta\omega}{k_s + F'(z_0)}. \tag{19}$$

We now consider that the sample contact stiffness constant may vary from point to point on the sample surface. We assume that the value of the sample contact stiffness constant k_s' at a given point on the surface differs from the value k_s at another position as $k_s' = k_s + \Delta k_s$. The value of the phase factor resulting from the change in the contact stiffness constant is obtained by substituting the value of k_s' into Eq. (19) to obtain

$$\beta_{cs}' = \tan^{-1}\frac{\gamma_s\Delta\omega}{k_s + F'(z_0) + \Delta k_s}. \tag{20}$$

For small values of Δk_s Eq. (20) may be expanded in a power series about $\Delta k_s = 0$ to obtain

$$\beta_{cs}' = \beta_{cs} + \Delta\beta_{cs}, \tag{21}$$

where

$$\Delta\beta_{cs} = \left(\frac{d\beta_{cs}'}{d(\Delta k_s)}\right)_0 \Delta k_s$$

$$= -\left(\frac{\gamma_s\Delta\omega}{[k_s + F'(z_0)]^2 + \gamma_s^2(\Delta\omega)^2}\right)\Delta k_s. \tag{22}$$

The surface contributions also include those produced at the cantilever drive frequency ω_c and manifested in the difference-frequency signal via the nonlinear tip-surface interaction in a manner similar to that from the ultrasonic wave interaction. The resulting phase contribution may be obtained by considering that the cantilever-sample tip interaction obeys to a good approximation the damped harmonic oscillator equation given by Eq. (17), in which $\Delta\omega$ is replaced by the cantilever drive frequency ω_c. The solution of the equation results in a phase contribution α_{cc} to the difference frequency given as

$$\alpha_{cc} = \tan^{-1}\frac{\gamma_s\omega_c}{k_s + F'(z_0)}. \tag{23}$$

For materials having variations Δk_s in the sample contact stiffness constant k_s the variation $\Delta\alpha_{cc}$ in α_{cc} is given as

$$\Delta\alpha_{cc} = \frac{\gamma_s\omega_c}{[k_s + F'(z_0)]^2 + \gamma_s^2\omega_c^2}\Delta k_s. \tag{24}$$

Three other terms are obtained from the analytical model[15] that result from the mathematical details of the nonlinear interaction and are not easily ascertained from feasibility arguments. These terms are

$$\phi_{cs} \approx \tan^{-1}\frac{(\gamma_c k_s + \gamma_s k_{cp})(\Delta\omega) - \gamma_s m_c(\Delta\omega)^3 + F'(z_0)(\gamma_c + \gamma_s)(\Delta\omega)}{k_{cp}k_s - (m_c k_s + \gamma_c\gamma_s)(\Delta\omega)^2 + F'(z_0)[k_{cp} + k_s - m_c(\Delta\omega)^2]}, \tag{25}$$

where k_{cp} is the cantilever stiffness constant corresponding to the pth (linear or nonlinear) noncontact resonance mode of the cantilever having a frequency nearest $\Delta\omega$ and γ_c is the cantilever damping coefficient,

$$\phi_{cc} \approx \tan^{-1}\frac{(\gamma_c k_s + \gamma_s k_{cq})\omega_c - \gamma_s m_c\omega_c^3 + F'(z_0)(\gamma_c + \gamma_s)\omega_c}{k_{cq}k_s - (m_c k_s + \gamma_c\gamma_s)\omega_c^2 + F'(z_0)(k_{cq} + k_s - m_c\omega_c^2)}, \tag{26}$$

and

$$\phi_{ss} \approx \tan^{-1}\frac{(\gamma_c k_s + \gamma_s k_{cr})\omega_s - \gamma_s m_c\omega_s^3 + F'(z_0)(\gamma_c + \gamma_s)\omega_s}{k_{cr}k_s - (m_c k_s + \gamma_c\gamma_s)\omega_s^2 + F'(z_0)(k_{cr} + k_s - m_c\omega_s^2)}, \tag{27}$$

where k_{cq} and k_{cr} are the cantilever stiffness constants corresponding to the qth and rth noncontact resonance modes of the cantilever having frequencies nearest ω_c and ω_s, respectively. The variations in these terms resulting from variations in k_s are

$$\Delta\phi_{cc} = -\frac{A_{cc}}{B_{cc}}\Delta k_s, \tag{28}$$

where

$$A_{cc} = [\gamma_s k_{cq}^2 + 2F'(z_0)\gamma_s k_{cq} + F'(z_0)^2(\gamma_c + \gamma_s)]\omega_c$$
$$+ [\gamma_c^2\gamma_s - 2\gamma_s m_c(k_{cq} + F'(z_0))]\omega_c^3 + m_c^2\gamma_s\omega_c^5 \tag{29}$$

and

$$B_{cc} = \{[\gamma_c k_s + \gamma_s k_{cq} + F'(z_0)(\gamma_c + \gamma_s)]\omega_c - \gamma_s m_c\omega_c^3\}^2$$
$$+ \{[k_{cq} - m_c\omega_c^2 + F'(z_0)]k_s + F'(z_0)(k_{cq} - m_c\omega_c^2)$$
$$- \gamma_c\gamma_s\omega_c^2\}^2, \tag{30}$$

$$\Delta\phi_{ss} = -\frac{A_{ss}}{B_{ss}}\Delta k_s, \tag{31}$$

where

$$A_{ss} = [\gamma_s k_{cr}^2 + 2F'(z_0)\gamma_s k_{cr} + F'(z_0)^2(\gamma_c + \gamma_s)]\omega_s$$
$$+ [\gamma_c^2\gamma_s - 2\gamma_s m_c(k_{cr} + F'(z_0))]\omega_s^3 + m_c^2\gamma_s\omega_s^5 \tag{32}$$

and

$$B_{ss} = \{[\gamma_c k_s + \gamma_s k_{cr} + F'(z_0)(\gamma_c + \gamma_s)]\omega_s - \gamma_s m_c\omega_s^3\}^2$$
$$+ \{[k_{cr} - m_c\omega_s^2 + F'(z_0)]k_s + F'(z_0)(k_{cr} - m_c\omega_s^2)$$
$$- \gamma_c\gamma_s\omega_s^2\}^2; \tag{33}$$

and

$$\Delta\phi_{cs} = -\frac{A_{cs}}{B_{cs}}\Delta k_s, \tag{34}$$

where

$$A_{cs} = [\gamma_s k_{cp}^2 + 2F'(z_0)\gamma_s k_{cp} + F'(z_0)^2(\gamma_c + \gamma_s)](\Delta\omega)$$
$$+ [\gamma_c^2\gamma_s - 2\gamma_s m_c(k_{cp} + F'(z_0))](\Delta\omega)^3 + m_c^2\gamma_s(\Delta\omega)^5 \tag{35}$$

and

$$B_{cs} = \{[\gamma_c k_s + \gamma_s k_{cp} + F'(z_0)(\gamma_c + \gamma_s)](\Delta\omega)$$
$$- \gamma_s m_c(\Delta\omega)^3\}^2 + \{[k_{cp} - m_c(\Delta\omega)^2 + F'(z_0)]k_s$$
$$+ F'(z_0)[k_{cp} - m_c(\Delta\omega)^2] - \gamma_c\gamma_s(\Delta\omega)^2\}^2. \tag{36}$$

The total near-surface phase contribution $(\Omega_{tot} + \Delta\Omega_{tot})$ to the difference-frequency signal is[15]

$$\Omega_{tot} + \Delta\Omega_{tot} = (\beta_{cs} + \alpha_{cc} + \phi_{ss} - \phi_{cc} - \phi_{cs})$$
$$+ (\Delta\beta_{cs} + \Delta\alpha_{cc} + \Delta\phi_{ss} - \Delta\phi_{cc} - \Delta\phi_{cs}), \quad (37)$$

where the set of terms within the first parentheses on the right side of Eq. (37) is Ω_{tot} and the set within the second parentheses is $\Delta\Omega_{tot}$. The contribution $(\Omega_{tot}+\Delta\Omega_{tot})$ is added to the phase contribution $(-\theta)$ from the bulk wave to give the net phase contribution to the difference-frequency signal.

Hertzian contact theory provides that the isotropic sample contact stiffness k_s is related to the Young modulus E of the sample as[3,10]

$$k_s = 2r_c \left(\frac{1 - \nu_T^2}{E_T} + \frac{1 - \nu^2}{E} \right)^{-1}, \quad (38)$$

where E_T is the Young modulus of the cantilever tip, ν and ν_T are the Poisson ratios of the sample and cantilever tip, respectively, and r_c is the cantilever tip–sample surface contact radius. From Eq. (38) we obtain

$$\Delta k_s = \frac{2r_c(1 - \nu^2)}{E^2} \left(\frac{1 - \nu_T^2}{E_T} + \frac{1 - \nu^2}{E} \right)^{-2} \Delta E. \quad (39)$$

C. Signal output using lock-in amplifier phase detection

The phase terms $-\theta$ and $(\Omega_{tot}+\Delta\Omega_{tot})$, given by Eqs. (14) and (37), directly contribute to the net phase of the RDF-AFUM signal. The negative sign before θ occurs because the contribution from the ultrasonic bulk wave having frequency ω_s appears as the $-\omega_s$ component in the difference-frequency signal $\Delta\omega = (\omega_c - \omega_s)$. The phase output signal from the lock-in amplifier is proportional to[17] $-\sin(\Omega_{tot}+\Delta\Omega_{tot}-\theta) = -\sin(\Omega_{tot}+\chi+\Delta\Omega_{tot}+\Delta\chi)$. Thus, for $[2n-(1/2)]\pi < (\Omega_{tot}+\chi) < [2n+(1/2)]\pi$, where n is an integer, a negative value of $(\Delta\Omega_{tot}+\Delta\chi)$ at a given point in the image produces an increase in the phase output signal at that point, whereas for $[2n+(1/2)]\pi < (\Omega_{tot}+\chi) < [2n+(3/2)]\pi$ a negative value of $(\Delta\Omega_{tot}+\Delta\chi)$ at a given point produces a decrease in the signal. The changes in the lock-in amplifier phase output signal resulting from the phase shift $(\Delta\Omega_{tot}+\Delta\chi)$ provide the image contrast in RDF-AFUM using phase detection. We make no attempt to provide a feasibility argument for the changes in the RDF-AFUM amplitude due to changes in k_s or from embedded features.

IV. APPLICATION TO LARC™-CP2 POLYIMIDE FILMS

Some recently developed high performance polymers having low density, high strength, optical transparency, and high radiation resistance are under consideration for a variety of applications in hostile space environments. One such polymer is the LaRC™-CP2 polyimide. We consider here the application of RDF-AFUM to assess variations in the Young modulus of the polymer at the nanoscale.

A specimen of the LaRC™-CP2 polyimide polymer roughly 12.7 μm thick containing a monolayer of randomly distributed gold particles, roughly 10–15 nm in diameter and embedded roughly 7 μm beneath the specimen surface, was
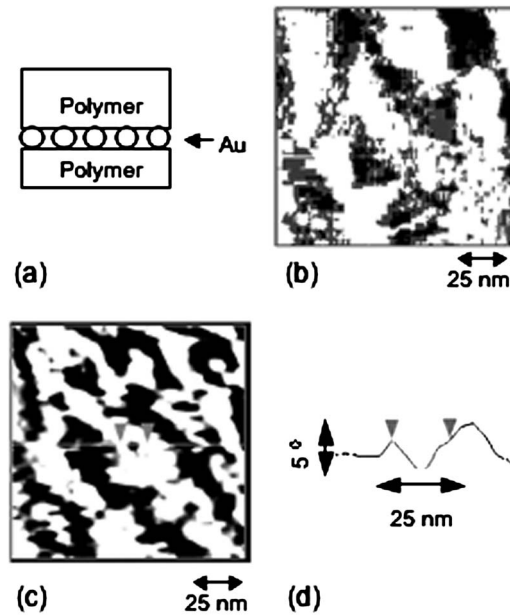

FIG. 2. Results obtained from 12.7 μm thick sample of LaRC™-CP2 containing a monolayer of gold particles (10–15 nm in diameter) 7 μm beneath the sample surface: (a) Depiction of specimen vertical cross section; (b) AFM intermittent soft contact image of sample surface; (c) RDF-AFUM phase image of the sample in the region coincident with the image of (b); (d) line scan of phase signal vs position across the center of the micrograph [indicated by the solid line in (c)]. The arrows frame the region around a gold particle.

imaged using both AFM intermittent soft contact mode and RDF-AFUM. The images are shown in Fig. 2. Figure 2(a) is a schematic of the specimen vertical cross section. Figure 2(b) is an AFM intermittent soft contact mode image using phase detection. A commercial cantilever, having a stiffness constant of 14 N m^{-1} and a lowest-mode resonance frequency of 302 kHz, is driven at 2.1 MHz in soft contact with the sample surface to obtain the micrograph of Fig. 2(b). Since no bulk ultrasonic wave is involved in the image, contrast results only from variations in the specimen near-surface sample stiffness constant k_s. The darker areas in the image correspond to larger values of the sample stiffness constant relative to that of the brighter areas. The maximum phase difference between the bright and dark areas in the image is approximately 1.5°.

A RDF-AFUM phase image of the same scan area as that of Fig. 2(b) is shown in Fig. 2(c). The RDF-AFUM image reveals bright and dark regions over the scan area that broadly correspond to the bright and dark regions in the surface image of Fig. 2(b), although the local detail appears to differ in the two images. The maximum variation in phase shown in Fig. 2(c) is approximately 13.2°. The values of the relevant model parameters for the LaRC™-CP2 polyimide polymer are[10,18,19] 1.4×10^3 kg m^{-3} for the mass density ρ, 2.4 GPa for the Young modulus E, 0.37 for the Poisson ratio ν, and roughly 10^{-8} kg s^{-1} for the cantilever damping coefficient. The value of $F'(z_0)$ that maximizes the difference-frequency signal is found from the frequency shifts of the cantilever resonances as a function of small applied loads corresponding to the soft contact nonlinear interaction force regime. $F'(z_0)$ is assessed to be roughly -53 at the tip-

surface separation corresponding to the maximum difference-frequency signal. It is important to recognize that large loads, corresponding to the hard contact regime, lead to nonlinear bending moments of the cantilever that induces additional frequency shifts quite apart from that of the tip-surface interaction forces.

The magnitude of $F'(z_0)$ is used to obtain from the experimental force-separation curve an estimated value of 0.8 μN for the adhesive force F_0 of the cantilever tip–sample surface interaction. The values of 17 nm for the cantilever tip–sample surface contact radius r_c and 96 N m^{-1} for the stiffness constant k_s are obtained from the Hertzian equations $k_s = (6E^{*2}RF_0)^{1/3}$ and $r_c = (3F_0R/4E^*)^{1/3}$, where $(E^*)^{-1} = [(1-\nu_T^2)E_T^{-1} + (1-\nu^2)E^{-1}]$, using the estimated value of F_0. The value of the cantilever tip radius R is varied in the Hertzian equations to optimize simultaneously the calculated variations of the RDF-AFUM and the intermittent contact mode phase signals[15] with respect to the measured phase variations of the respective techniques over the same scan area of the specimen. Optimization occurs in the present experiment for the value $R = 24$ nm. An estimated value of 4.8 $\times 10^{-5}$ kg s^{-1} for the damping coefficient γ_s is obtained from the relationship derived in Ref. 15 between the damping coefficient and the ultrasonic attenuation using the measured value for the ultrasonic attenuation α of roughly 85 Np m^{-1}.

From the above parameter values we calculate from Eqs. (5), (15), (19), (23), and (25)–(27) that $\Omega_{tot} + \chi$ has the value of 3.53. Electronic phase contributions are zeroed out before the cantilever engages the sample surface. Hence, $\pi/2 < (\Lambda_{tot} + \chi) < 3\pi/2$ for the RDF-AFUM imaged sample of LaRC™-CP2. According to the results of Sec. III C such a value of $(\Omega_{tot} + \chi)$ means that a negative value of $(\Delta\Lambda_{tot} + \Delta\chi)$ at a given point produces a decrease in the phase signal. From Eqs. (7), (16), and (37) a negative value of $(\Delta\Lambda_{tot} + \Delta\chi)$ means that ΔE and Δc are positive. Thus, the darker regions in the phase detected RDF-AFUM image correspond to regions of larger elastic moduli than that of the brighter regions.

The existence of a contiguous material with differing elastic constants suggests that the LaRC™-CP2 material is not homogeneous. The broad coincidence of dark (bright) regions in the images of Figs. 2(b) and 2(c) further suggests that the polymer structure giving rise to a larger (smaller) elastic modulus in the bulk material occurs in varying amounts through the bulk to the surface, the degree of darkness (brightness) in Fig. 2(c) being somewhat reflective of the structural homogeneity of the material along the propagation path of the ultrasonic wave. If we assume that the darkest and the brightest regions in Fig. 2(c) each corresponds to the bulk material in which a given polymer structure is homogeneous through the thickness of the material, then we may use the model developed in Sec. III to estimate the variation in the Young modulus resulting from the variation in the polymer structure. Using the above parameter values in the expression for $(\Delta\Omega_{tot} + \Delta\chi)$ and assuming $E_T \gg E$ in Eq. (39), we calculate that for a measured variation of 13.2° in the RDF-AFUM phase image of Fig. 2(c) the frac-

tional change in the ultrasonic velocity, $\Delta c/c$, is approximately 12% and that the fractional variation in the Young modulus, $\Delta E/E$, is roughly 24%.

We also see in the RDF-AFUM phase image of Fig. 2(c) the appearance of circular dark features, approximately 10–15 nm in diameter. These features are most noticeable against the bright fields in the micrograph and correspond roughly to the size of the gold particles randomly distributed 7 μm below the sample surface. Figure 2(d) is a line scan from the central region of the micrographs [indicated by the line in Fig. 2(c)] giving the phase variation of the RDF-AFUM signal plotted as a function of cantilever tip position on the sample surface. The region between the arrows in Figs. 2(c) and 2(d) is thought to show the effects of a gold particle.

The magnitude of the phase variations associated with spherical gold nanoparticles may be calculated from Eqs. (7) and (16) using the value $d/2 = 15$ nm, corresponding to the largest diameter of the gold particles, and $c_d = 5.1 \times 10^3$ m s^{-1} for the longitudinal ultrasonic phase velocity of the gold particles. The magnitude of the RDF-AFUM phase variation from the embedded nanoparticle is calculated to be of the order of 10^{-3} deg. This phase variation is much smaller than the 2°–3° variation shown in the line scan in Fig. 2(d) and suggests that the presence of the embedded gold particle may induce a local change in the matrix material surrounding the particle that leads to the larger measured phase shift of 2°–3° for the region between the arrows.

The phase shift contribution from the wave propagation alone through a region of the bulk LaRC™-CP2 material in which the variation in ultrasonic velocity is 12% is calculated to be of the order of 0.1°. The total contribution from particle and polymer matrix materials resulting from bulk wave propagation is again much smaller than the measured variation of 2°–3°. This implies that the manifestation of the particle effects in the RDF-AFUM micrograph likely results from variations in k_s at the specimen surface. A 2°–3° variation in the RDF-AFUM micrograph would correspond to a 0.2°–0.3° variation in the intermittent soft contact mode image. Such a variation would be more difficult to see clearly in the intermittent soft contact mode micrograph since the image contrast in Fig. 2(b) is considerably weaker than that of Fig. 2(c). Nonetheless, a careful examination of Fig. 2(b) also shows the appearance of some circular objects that are coincident with that of Fig. 2(c).

Assuming that the circular object in the RDF-AFUM micrograph is a gold nanoparticle, we note that the region around the particle shows a steady decrease in the RDF-AFUM phase signal [Fig. 2(d)] as the particle is approached. This indicates that the elastic modulus grows larger with decreasing distance from the particle in that region and suggests that the presence of the gold particles may stimulate a preferential growth of a particular material phase (presumably a crystalline phase) during the curing of the LaRC™-CP2 polyimide polymer. Such growth may result from internal stresses generated during curing by the different thermal expansion coefficients of the gold and polymer materials. This conjecture is consistent with the preferential growth of crystalline phases following the mechanical stretching of

LaRC™-CP2 sheet samples in which the Young modulus is measured to vary by 21% between the amorphous phase (before stretching) and the crystalline phase (after stretching).[18] This variation in the Young modulus is also consistent with the value of 24% calculated from the present RDF-AFUM measurements and analytical model.

V. CONCLUSION

The above results show that RDF-AFUM can be used to obtain images of nanoscale subsurface features without the need to make any modifications to the AFM itself. The technique requires only the addition of off-the-shelf instrumentation for implementation and takes advantage of ultrasonic-range probing signals propagating through the bulk of the sample. The analytical development of Sec. III provides a means for obtaining a quantitative measure of the variations in the sound velocity and the Young modulus of the imaged material from variations in the RDF-AFUM phase detected output signal. Although similar information can be obtained from the intermittent contact mode phase image from variations in k_s, the RDF-AFUM micrograph produces larger amplitude phase variations (13.2° for the present material) than the intermittent contact mode (1.5°) that permits a greater image contrast. Unlike intermittent soft contact mode imaging, the RDF-AFUM also allows the imaging of subsurface structures, although the structures may be obscured in the presence of strong near-surface features.

The application of the analytical model to RDF-AFUM measurements of a 12.7 μm thick sample of the LaRC™-CP2 polyimide polymer containing a monolayer of gold nanoparticles embedded 7 μm below the sample surface reveals maximum fractional changes of 12% and 24%, respectively, for the sound velocity and Young modulus of the material. The present calculation of 24% for the variation in the Young modulus of LaRC™-CP2 is in agreement with a value of 21% obtained from mechanical stretching experiments in which the increase in the modulus is attributed to the growth during stretching of a crystalline phase having a larger Young modulus than that of the original amorphous phase.[18]

Line scans (for which Fig. 2(d) is one example) from the RDF-AFUM micrograph also suggest the presence a crystalline phase of LaRC™-CP2 in the immediate region around each of the gold particles. Although the total phase variation from an individual particle and surrounding matrix material is quite small (roughly 0.1°), a much larger variation [roughly 2°–3° in Fig. 2(d)] is obtained from the effects of the nanoparticle at the specimen surface. Considerations of the scale of Fig. 2(d) and the distance of the particle beneath the specimen surface imply that the effects of the embedded particle are manifested at a much greater distance in the vertical direction than in the horizontal plane of the RDF-AFUM micrograph. If so, this would imply a preferred crystallization and growth direction during the curing of the LaRC™-CP2 film.

Assuming that the circular objects in Fig. 2(c) are indeed embedded gold nanoparticles, we find that the phase increases with distance from the nanoparticle. This indicates for the present RDF-AFUM parameters a decrease in the Young modulus. In view of the mechanical stretching experiments[18] such a variation in the Young modulus is consistent with the presence of a crystalline phase surrounding the gold nanoparticle. The growth of crystalline phases around the embedded particles may be initiated locally by internal stresses generated during curing by the different thermal expansion coefficients of the gold and polymer materials.

A more complete understanding of the nonlinear cantilever tip–sample surface interactions responsible for the generation of the difference-frequency signals and the resulting image contrast would be helpful in the interpretation and more quantitative exploitation of RDF-AFUM micrographs. A comprehensive analytical model of cantilever dynamics in the nonlinear interaction region has been developed. It provides such information not only for RDF-AFUM but for a variety of acoustic-atomic force microscopy modalities including the AFM intermittent hard and soft contact modes. A manuscript on the analytical model is presently in preparation for journal submission.

[1] G. Binnig, C. F. Quate, and Ch. Gerber, Phys. Rev. Lett. **56**, 930 (1986).
[2] U. Rabe and W. Arnold, Appl. Phys. Lett. **64**, 1493 (1994).
[3] U. Rabe, K. Janser, and W. Arnold, Rev. Sci. Instrum. **67**, 3281 (1996).
[4] D. C. Hurley, K. Shen, N. M. Jennett, and J. A. Turner, J. Appl. Phys. **94**, 2347 (2003).
[5] U. Rabe, S. Amelio, M. Kopychinska, S. Hirsekorn, M. Kempf, M. Goken, and W. Arnold, Surf. Interface Anal. **33**, 65 (2002).
[6] K. Yamanaka, H. Ogiso, and O. Kolosov, Appl. Phys. Lett. **64**, 178 (1994).
[7] R. E. Geer, O. V. Kolosov, G. A. D. Briggs, and G. S. Shekhawat, J. Appl. Phys. **91**, 9549 (2002).
[8] O. V. Kolosov, M. R. Castell, C. D. Marsh, and G. A. D. Briggs, Phys. Rev. Lett. **81**, 1046 (1998).
[9] L. Muthuswami and R. E. Geer, Appl. Phys. Lett. **84**, 5082 (2004).
[10] G. G. Yaralioglu, F. L. Degertekin, K. B. Crozier, and C. F. Quate, J. Appl. Phys. **87**, 7491 (2000).
[11] M. T. Cuberes, H. E. Alexander, G. A. D. Briggs, and O. V. Kolosov, J. Phys. D **33**, 2347 (2000).
[12] G. S. Shekhawat and V. P. Dravid, Science **310**, 89 (2005).
[13] Y. Zheng, R. E. Geer, K. Dovidenko, M. Kopycinska-Müller, and D. C. Hurley, J. Appl. Phys. **100**, 124308 (2006).
[14] H. Überall, in *Encyclopedia of Acoustics*, edited by M. J. Crocker (Wiley, New York, 1997), Vol. 1, p. 55.
[15] J. H. Cantrell and S. A. Cantrell (unpublished).
[16] D. I. Bolef and J. G. Miller, in *Physical Acoustics*, edited by W. P. Mason and R. N. Thurston (Academic, New York, 1971), Vol. VIII, pp. 95–201.
[17] P. Horowitz and W. Hill, *The Art of Electronics* (Cambridge University Press, New York, 1980).
[18] C. C. Fay, D. M. Stoakley, and A. K. St. Clair, High Perform. Polym. **11**, 145 (1999).
[19] C. Park *et al.*, Chem. Phys. Lett. **364**, 303 (2002).